PERGAMON

Continental Shelf Research 21 (2001) 1299–1315

CONTINENTAL SHELF RESEARCH

www.elsevier.com/locate/csr

Note

Objective analysis for coastal regimes

Daniel R. Lynch[a,*], Dennis J. McGillicuddy Jr.[b]

[a] *Dartmouth College, Hanover NH 03755-8000, USA*

[b] *Woods Hole Oceanographic Institution, Woods Hole, MA 02543, USA*

Received 19 July 2000; accepted 23 January 2001

Abstract

Statistical interpolation of coastal oceanic fields is addressed within the general framework of Gauss–Markov estimation. Computation of the prior covariance of the field to be estimated is posed as a stochastically-forced differential equation subject to coastal boundary conditions with inhomogeneous, anisotropic parameters. Solution is readily implemented in standard finite element methodology. Examples illustrate the method for idealized one-dimensional situations. Analysis of real biological data from Massachusetts and Cape Cod Bay is shown, using a covariance function derived from velocity and diffusivity fields computed with a hydrodynamic model. The procedure defaults to standard OA methods using distance-based covariance functions, far from boundaries and inhomogeneities.

Keywords: Gauss–Markov estimation; Statistical interpolation; Finite element

1. Introduction

Objective analysis (OA) is a contemporary synonym for statistical estimation based on the Gauss–Markov theorem. This theorem provides a sound basis for interpolation of irregularly spaced data. It was introduced to meteorology by Gandin (1963) and is widely used operationally. Bretherton et al. (1976) introduced the theory to oceanography in the context of the Mid-Ocean Dynamics Experiment. Good theoretical descriptions are provided by Daley (1991) and Wunsch (1996).

The general theory requires a prior statistical description of the field being estimated, and of the observational error or noise. Knowledge of the field statistics does not come easily in oceanography, owing to the relative paucity of observations. Practical procedures try to fit

*Corresponding author. Fax: +1-603-646-3856.

E-mail address: d.r.lynch@dartmouth.edu (D.R. Lynch).

0278-4343/01/$ - see front matter
PII: S0278-4343(01)00007-3

simple analytic covariance functions to data. Almost universally, these are spatially homogeneous, isotropic functions with a small (1 or 2) number of degrees of freedom. It is widely recognized that this is a potentially serious limitation, especially in coastal regions and shelf seas. In these areas, topography (bathymetry and coastline), local dynamics and transport processes exert strong local influences on oceanographic fields; and the assumptions of homogeneity and isotropy are basically inappropriate. Under these conditions, the prior knowledge is defective and the analysis is compromised.

In this paper we develop a general approach to OA which relieves some of these deficiencies. The central idea is the numerical construction of the field covariance in a way which recognizes local variations and the coastal constraint. The approach involves posing these influences via a discretized partial differential equation subject to stochastic forcing.

2. General theory

We wish to map an irregular array of observations $\{d\}$ to an unstructured computational grid of values $\{u\}$ representing realistic coastal geometries. The base theory is Gauss–Markov estimation. This theory treats the general linear mapping

$$\{u\} = [B]\{d\} \tag{1}$$

which is optimal (i.e. $u = \tilde{u}$) when the estimator $[B]$ is given by

$$[B] = [C_{ud}][C_{dd}]^{-1} \tag{2}$$

with $[C_{ab}]$ the covariance matrix among arrays $\{a\}$ and $\{b\}$. $[B]$ is a minimum variance estimator. If $\{u\}$ and $\{d\}$ have zero means, $[B]$ is unbiased ("Best Linear Unbiased Estimator", Wunsch, 1996, p. 183; Bennett, 1992, p. 48.) The precision of the optimal estimate $\tilde{u}$ is given by its covariance $C_{\tilde{u}\tilde{u}}$:

$$[C_{\tilde{u}\tilde{u}}] = [C_{uu}] - [B][C_{ud}^*] = [C_{uu}] - [C_{ud}][C_{dd}]^{-1}[C_{ud}^*]. \tag{3}$$

(Here and throughout, C^* indicates the transpose of C.)

We are especially interested in mapping $\{d\}$ onto a continuous finite element representation $u(x, y)$ with finite number of degrees of freedom u_i:

$$u(x, y) = \sum_i u_i \phi_i(x, y), \tag{4}$$

where $\phi_i(x, y)$ are the finite element (FE) basis functions providing a unique interpolant among the nodal values u_i of an FE grid. Sampling this function at the observation points gives

$$[E]\{u\} + \{n\} = \{d\}, \tag{5}$$

where $[E]$ is a measurement operator incorporating interpolation of the ϕ to the observation points and local averaging appropriate to the data; and $\{n\}$ is observational noise.[1] Assuming signal $\{u\}$ and noise $\{n\}$ to be uncorrelated, we have

$$[C_{ud}] = [C_{uu}][E^*] \text{ and } [C_{dd}] = [E][C_{uu}][E^*] + [C_{nn}] \tag{6}$$

[1] More precisely, n is the model–data misfit, which will be a priori ascribed to observational noise.

and the optimal estimate is

$$\{\tilde{u}\} = [C_{uu}][E^*][[E][C_{uu}][E^*] + [C_{nn}]]^{-1}\{d\} \tag{7}$$

or, equivalently (Wunsch, 1996, p. 184)

$$[[C_{uu}]^{-1} + [E^*][C_{nn}]^{-1}[E]]\{\tilde{u}\} = [E^*][C_{nn}]^{-1}\{d\}. \tag{8}$$

The precision of the estimate $\tilde{u}$ is given by[2]

$$[C_{\tilde{u}\tilde{u}}] = [C_{\tilde{u}\tilde{u}}] - [B][C^*_{ud}] = [C_{uu}] - [B][E][C^*_{uu}]. \tag{9}$$

The key to objective analysis, then, is knowledge of $[C_{uu}]$ and $[C_{nn}]$, the signal and noise covariances. Computing $[C_{uu}]$ is our main interest.

3. Covariance and stochastically forced differential operators

Classically, the covariance of the underlying field $[C_{uu}]$ has been expressed in simple analytical forms with a few degrees of freedom, leading to practical procedures as in Bretherton et al. (1976). Typical are covariances of the form $C(r)$, where r is scaled distance separating any two points.

Freeland and Gould (1976) estimated streamfunction from velocity measurements in the Mid-Ocean Dynamics Experiment. Isotropic, homogeneous covariance functions $C_{\psi\psi}(r)$, $C_{uu}(r)$, $C_{vv}(r)$ describe the streamfunction and the longitudinal and transverse[3] velocity covariances, as functions of the spatial separation distance r. Constraining these functions are the physical relations defining them (non-divergent, geostrophic flow) and several constraints representing statistical realizability. The forms chosen are

$$C_{uu}(r) = (1 + br)\mathrm{e}^{-br}, \tag{10}$$

$$C_{vv}(r) = (1 + br - b^2r^2)\mathrm{e}^{-br}, \tag{11}$$

$$C_{\psi\psi}(r) = (1 + br + b^2r^2/3)\mathrm{e}^{-br}. \tag{12}$$

Thus we have one-parameter, homogeneous isotropic covariances. The MODE data were used to estimate b. McWilliams (1976) made similar estimates using MODE data, assuming geostrophic, non-divergent flow and homogeneous, isotropic covariance. Two-parameter functions were fitted to the data:

$$C_{\psi\psi}(r) = (1 - \gamma^2r^2)\mathrm{e}^{-\delta^2r^2/2}, \tag{13}$$

$$C_{uu}(r) = (1 - b^2r^2)\mathrm{e}^{-\delta^2r^2/2}, \tag{14}$$

$$C_{vv}(r) = (1 - [5 + \delta^2/\gamma^2]b^2r^2 + \delta^2b^2r^4)\mathrm{e}^{-\delta^2r^2/2} \tag{15}$$

with the constraint $b^2 = \gamma^2\delta^2/(\gamma^2 + \delta^2)$.

Denman and Freeland (1985) estimated two-parameter covariance functions from observations over the continental shelf west of Vancouver Island. Fitted functions are reported for geopotential

[2] Typically, $u \approx \tilde{u} \pm S$, where S^2 is the diagonal of $[C_{\tilde{u}\tilde{u}}]$.

[3] The directions are relative to the separation vector r.

height and velocity under similar assumptions as Freeland and Gould (1976), plus temperature, salinity, and chlorophyll. Functional forms used included

$$C(r) = (1 - r^2/b^2)\mathrm{e}^{-r^2/a^2}, \tag{16}$$

$$C(r) = \cos(r/b)\mathrm{e}^{-r^2/a^2}, \tag{17}$$

$$C(r) = J_0(r/b)\mathrm{e}^{-r^2/a^2} \tag{18}$$

(J_0 is the Bessel function of the first kind.) Good fits to several of these two-parameter forms were found; but the data were insufficient to support the estimation of anisotropic covariance functions suitable for the shelf.

Hendry and He (2000) implemented OA for shelf estimations using the covariance function as in Freeland and Gould (1976)

$$C_{uu}(\rho) = (1 + \rho + \rho^2/3)\mathrm{e}^{-\rho}. \tag{19}$$

In that implementation, ρ is an anisotropic, space-time pseudo-distance, with principal axes and scaling defined locally, prior to the data. Several studies of the Gulf of Maine/Scotian Shelf region, including Naimie et al. (1994), Lynch et al. (1996), Hannah et al. (1996), Loder et al. (1997) and McGillicuddy et al. (1998) have used this procedure to estimate hydrographic and biological fields. In those cases the local correlation axes were keyed to the local bathymetric gradient with longer correlation scales along isobaths than across them.

Zhou (1998) studied space–time interpolation of plankton data, using the covariance function

$$C(\rho) = (1 - \rho)\mathrm{e}^{-\rho}, \tag{20}$$

where again ρ is a scaled pseudo-distance, in this case involving an isotropic two-dimensional spatial scale and a temporal scale. This form was fit to the observed data. A key idea is the Lagrangian correction of the spatial distribution. The observations were passively advected either forward or backward to a common time, in an attempt to offset the spatial distortion associated with the non-synoptic sampling. Following this advective adjustment, the correlation function (20) was spatially isotropic and homogeneous. The advective field was itself based on geostrophic diagnosis of objectively analyzed hydrography.

These types of covariance functions have served well in the studies cited. But in the coastal regime, there are serious complications:

- *coastline constraints*: there is no direct distance relationship across landforms (islands, peninsulas),
- *anisotropy*: advection creates locally anisotropic covariance, oriented to streamlines; other dynamical processes may be oriented by the local bathymetric gradient,
- *inhomogeneity*: correlation scales and principal axes may vary locally, reflecting for example differential mixing or advective regimes.

Practical incorporation of these effects into $[C_{uu}]$ is our goal.

Our basic idea is to represent the underlying variability as the outcome of a stochastic process; specifically, the result of a stochastically forced differential equation (SDE). For example, the

simple equation

$$\frac{\partial^2 u}{\partial x^2} - k^2 u = \varepsilon(x) \tag{21}$$

with the *process noise* ε a (0,1) random disturbance with no spatial correlation, has covariance

$$C_{uu}(r) = (1 + kr)\mathrm{e}^{-kr} \tag{22}$$

when posed in an unbounded domain. Thus Eqs. (21) and (22) are equivalent statements of the same problem. The 2-D pair

$$\nabla^2 u - k^2 u = \varepsilon(x, y), \tag{23}$$

$$C_{uu}(r) = krK_1(kr) \simeq \left(\frac{\pi}{2}kr\right)^{1/2}\left(1 + \frac{3}{8kr}\right)\mathrm{e}^{-kr}, \quad kr \to \infty \tag{24}$$

are likewise equivalent statements (Balgovind et al., 1983). (K_1 is the Bessel function of the second kind.)

The importance of the SDE approach is that C_{uu} can be computed numerically for realistic conditions — real topography, variable coefficients and resolution, boundary conditions—which make analytic solutions impossible. And, the parameters and process noise model ε can be chosen to represent real processes affecting the field of interest. And, the limiting case, far from boundaries and inhomogeneities, defaults to an equivalent $C(r)$ structure. Balgovind et al. (1983) used the SDE approach (specifically, the Helmholtz equation (23) with k^2 varying with latitude) to compute a realistic spatially varying covariance for meteorological forecast error. Here we use it to analyze coastal oceanic fields.

Discretization of Eqs. (21) and (23) or any other differential operator on a finite element grid leads to the matrix form

$$[A]\{u\} = \{e\} \tag{25}$$

in which all coastal constraints (no transport across land boundaries) are incorporated automatically. The covariance of the FE nodal variables is obtained directly:

$$[C_{uu}] = [A]^{-1}[C_{ee}][A]^{-1*}, \tag{26}$$

$$[C_{uu}]^{-1} = [A^*][C_{ee}]^{-1*}[A] \tag{27}$$

Immediately we have accounted, formally, for (a) realistic transport processes and BCs in $[A]$, and (b) realistic process errors in C_{ee}, representing processes not modeled in $[A]$ or in the prior estimate. Knowledge of these two effects allows us to compute $[C_{uu}]$ using standard finite element solution techniques. Coupling Eq. (26) with Eqs. (7)–(9), we have objective analysis. This is the central idea of this paper.[4]

Aside, note that use of Eqs. (7)–(9), with $[C_{uu}]$ from Eq. (26) is equivalent to solving the weighted least squares problem

$$\text{Minimize } \{\{n\}^*[C_{nn}]^{-1}\{n\} + \{e\}^*[C_{ee}]^{-1}\{e\}\} \tag{28}$$

[4] Two examples follow in Section 4 and 5.

subject to the constraints (5) and (25) which define the model–data mismatch n and the process noise e (Wunsch, 1996).

4. Example 1

Consider the SDE

$$\frac{\mathrm{d}}{\mathrm{d}x} D \frac{\mathrm{d}u}{\mathrm{d}x} + V \frac{\mathrm{d}u}{\mathrm{d}x} - k^2 u = \varepsilon \tag{29}$$

and its discretization (assuming constant D)

$$[1 - P_e]u_{i-1} - [2 + K^2]u_i + [1 + P_e]u_{i+1} = E_i \tag{30}$$

with dimensionless quantities

$$P_e = \frac{Vh}{2D}, \qquad K^2 = \frac{k^2 h^2}{D}, \qquad E = \frac{\varepsilon h^2}{D} \tag{31}$$

$[A]$ is tridiagonal; $[A^*][A]$ is pentadiagonal with columns

$$\left\{ \begin{array}{c} 0 \\ \vdots \\ 0 \\ (1 - P_e^2) \\ -2(2 + K^2) \\ 2(1 + P_e^2) + (2 + K^2)^2 \\ -2(2 + K^2) \\ (1 - P_e^2) \\ 0 \\ \vdots \\ 0 \end{array} \right\}. \tag{32}$$

The inverse of $[A^*][A]$, assuming $[C_{EE}] = [I]$, gives the covariance C_{uu}. This will be a full matrix, with the covariance structure centered on the diagonal. It is plotted in Figs. 1 and 2, assuming periodic boundary conditions. Note that $K = 1/N$, where N is the number of grid cells per e-folding length for the analytic solution; thus a reasonable discretization has $K = \mathrm{O}(1)$ or less. Similarly, $P_e = 1$ is a threshold for poor resolution of advection and accompanies loss of diagonal dominance in the case $K^2 = 0$.

In Fig. 1 we show C_{uu} with periodic BCs, for $P_e = 0$. From Eq. (22) we expect the decorrelation scale to be $1/K$ grid cells. Fig. 1 confirms that for large K we have essentially an unbounded domain. Decreasing K broadens the covariance. Fig. 1 also confirms that for large K we recover the analytical result; while at small K ($=0.01$ in this example) the BCs have effect and the free-space analytic solution becomes invalid.

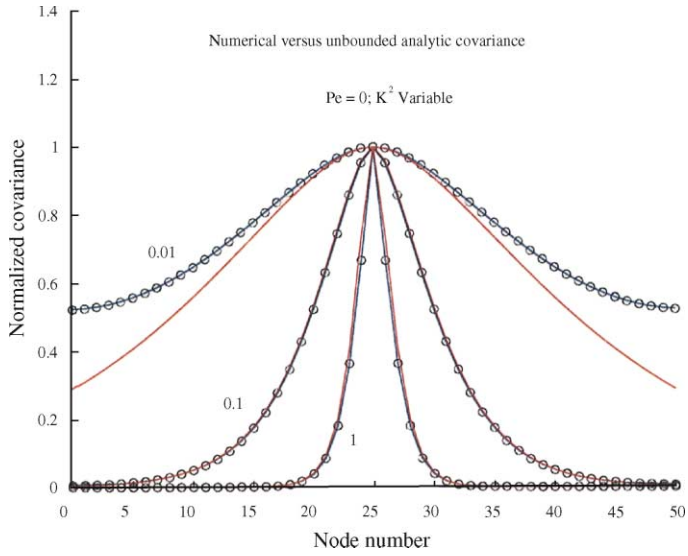

Fig. 1. Covariance for the advective–diffusive–reactive equation (30) with periodic boundary conditions (blue, dots), compared with the analytic free-space result (red, solid). Three different values of K^2 are shown. The plots have been self-normalized.

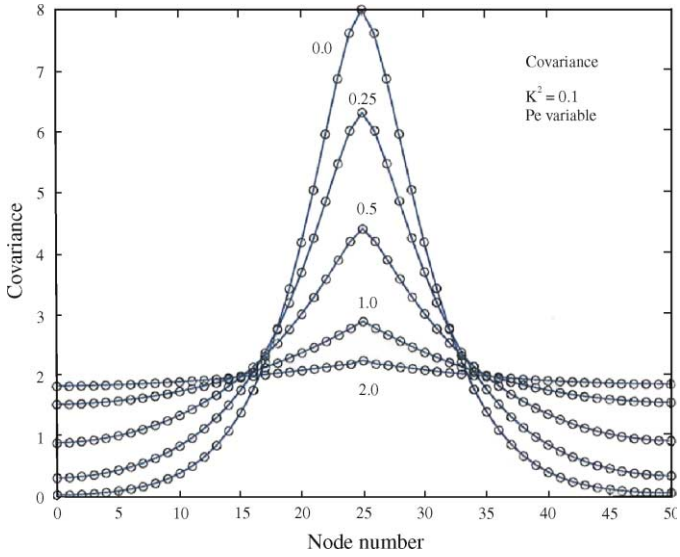

Fig. 2. Covariance for the advective–diffusive–reactive equation, for five values of P_e. Periodic BCs.

Fig. 2 shows C_{uu}, again with periodic BCs, for various values of P_e. The effect of advection is to lengthen the correlation scale, increasing covariance in the along-stream direction. In the steady state, the upstream and downstream effects are symmetric. Creative use of these two parameters sets a baseline correlation scale via K and directional anisotropy via P_e, both of which can be locally variable. Modulation near shoreline boundaries is naturally incorporated from the outset.

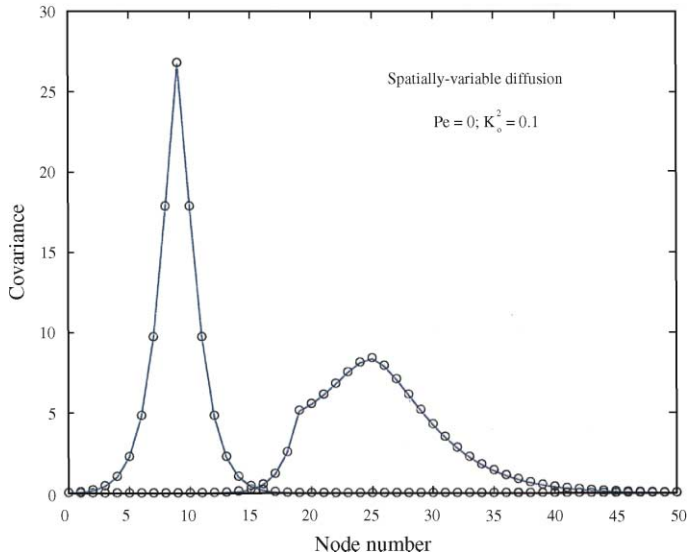

Fig. 3. Effect of variable diffusion coefficient on covariance. To the left of node 19, $D = D_0/10$; to the right, $D = D_0$. The two curves are associated with nodes 10 (left curve) and 25 (right curve). Periodic BCs; $P_e = 0$; $K_0^2 = 0.1$.

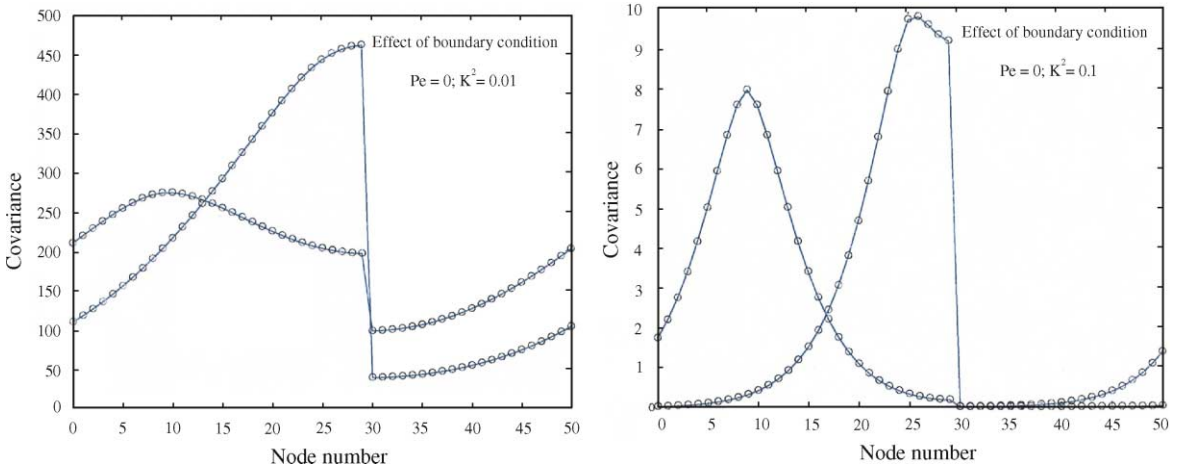

Fig. 4. Effect of no-flux boundary condition between nodes 30 and 31 on covariance with nodes 10 (left curves) and 25 (right curves). Periodic BCs; $P_e = 0$; $K^2 = 0.01$ (left) and 0.1 (right).

In Fig. 3 we show the effect of a spatial variation in diffusion coefficient. In this case, there is a step change by a factor of 10 in D at node 19. The result is asymmetry (right curve) and inhomogeneity (left curve versus right) in the covariance. Fig. 4 shows the result of an impermeable land boundary between nodes 31 and 32. Disturbances introduced near this boundary must diffuse around it by a much longer path; thus the covariance of geographic near-neighbors is greatly reduced.

These results illustrate local control of the correlation length scales using physical parameters and boundary conditions of the underlying differential equation.

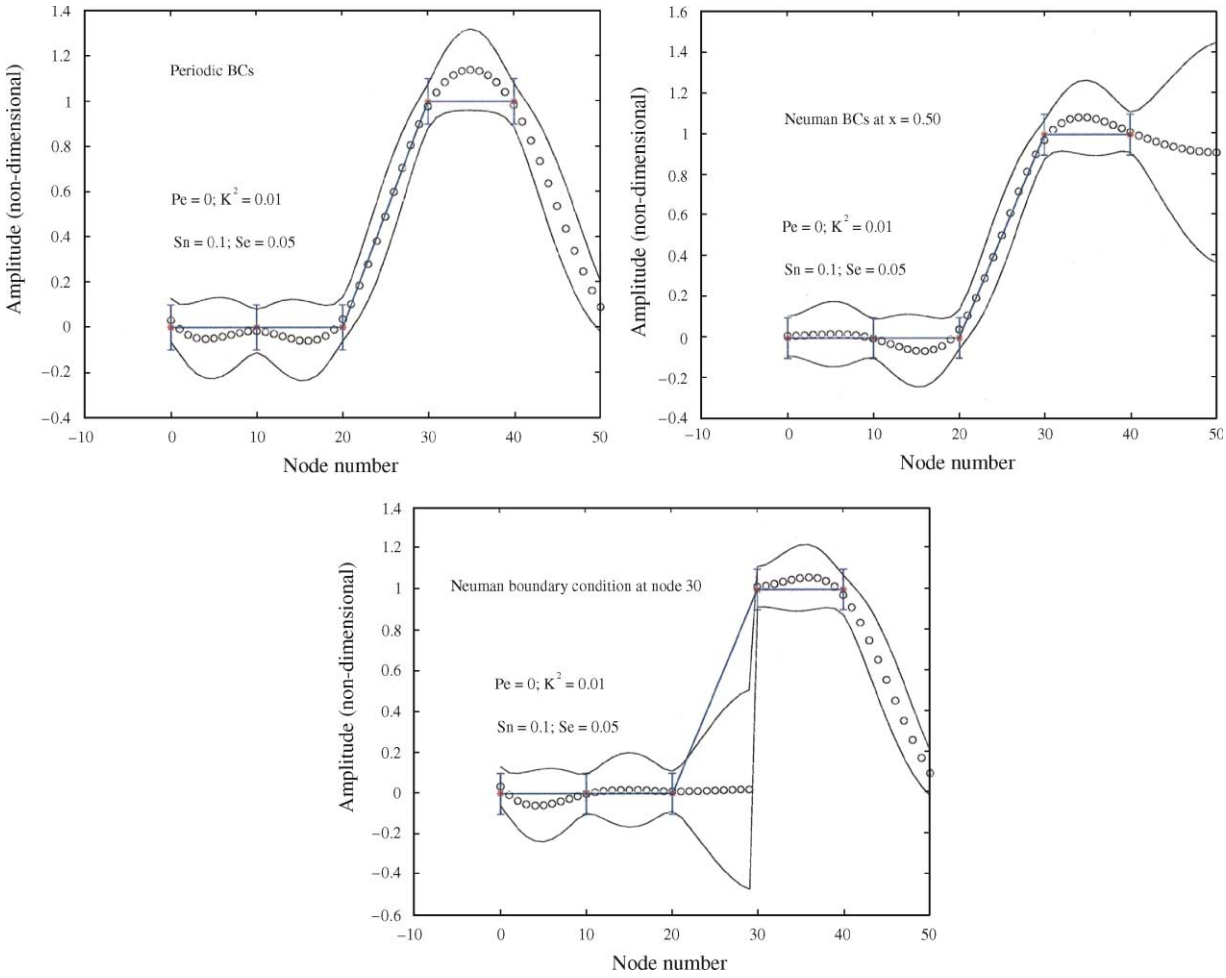

Fig. 5. Objective analysis of five data with various boundary conditions. The data (red asterisks) are connected by a solid blue line representing simple linear interpolation. The OA estimates are indicated by the circles. The standard deviations of the data (blue error bars) and of the estimated interpolant (black solid lines) are also shown. Top left: periodic BCs at left and right. Top right: Neumann BCs at left and right. Bottom: Neumann BCs in center of domain (just left of Node 30) and periodic BC's at left and right. Standard deviations of observational noise S_n and process noise S_e are indicated. The top right and bottom panels illustrate the successful blocking of interpolation across a coastal boundary.

Objective analyses of five data sampled at intervals of $10\,\Delta x$ are plotted in Fig. 5. The three cases illustrate the significant variations among the interpolants, depending on the details of boundary conditions. Also shown are the estimated standard deviations of the interpolations and of the data. At Neumann boundaries, the interpolation is discontinuous and the interpolation uncertainty grows where data need to be extrapolated. Another effect of the internal Neumann boundary is the reduction of the interpolation maximum at node 35, due to its isolation from the data to the left (bottom panel of Fig. 5).

5. Example 2

Next we consider the 2-D transport equation

$$\frac{1}{h}\nabla \cdot hD\nabla u - \mathbf{V} \cdot \nabla u - k^2 u = \varepsilon_s + \varepsilon_p, \tag{33}$$

where u is the field anomaly, h the bathymetric depth, D the dispersion coefficient, $\mathbf{V}$ the fluid velocity, k^2 the first-order decay rate, ε_s the surface forcing, and ε_p the isolated inputs from point sources (e.g. river discharges).

We imagine for example that climatological estimates of all transport parameters are available, and that a climatological prior estimate of the transported field has been subtracted from the data. Standard Galerkin FE discretization leads to

$$[A]\{u\} = \{e_s\} + \{e_p\} + \{r\}, \tag{34}$$

$$A_{ij} = \langle -hD\nabla\phi_j \cdot \nabla\phi_i - h\mathbf{V} \cdot \nabla\phi_j\phi_i - hk^2\phi_j\phi_i \rangle, \tag{35}$$

$$r_i = -\oint hD\frac{\partial u}{\partial n}\phi_i, \tag{36}$$

$$e_{si} = \langle h\varepsilon_s\phi_i \rangle, \tag{37}$$

$$e_{pi} = \langle h\varepsilon_p\phi_i \rangle, \tag{38}$$

where $\langle\ \rangle$ indicates integration over the spatial domain, and $\oint$ integration over its boundary. The $\{e_s\}$ vector might be constituted as random noise plus a highly structured response correlated with weather; $\{e_p\}$ might be correlated with hydrological conditions or industrial activity.

To demonstrate the utility of this methodology, we applied it to a complex geometry in a coastal domain off Massachusetts. Velocity and diffusivity fields were specified from a simulation of the March–April climatological flow (Fig. 6). The basis of these simulations is a fully nonlinear, three-dimensional primitive equation model with turbulence closure (Lynch et al., 1996). This model has been used extensively to study coastal currents in this region, particularly in the area north of Cape Cod (Lynch et al., 1997). Archived solutions (see http://www-nml.dartmouth.edu/CircMods/) were vertically averaged to obtain D and $\mathbf{V}$ fields suitable for use in Eq. (33). The circulation is dominated by a southward flowing coastal current, which partially bifurcates south of Cape Ann. During this time period, a small portion of the current splits off and flows through Massachusetts and Cape Cod Bays. This branch subsequently rejoins the bulk of the coastal current off the northern tip of Cape Cod, where the southward flow intensifies (note that the fine mesh on the steep topography east of Cape Cod makes the current appear more intensified in Fig. 6 than it actually is). The highest diffusivities (in excess of $500\,m^2s^{-1}$) are associated with Martha's Vineyard and Nantucket islands south of Cape Cod; another local maximum (on the order of $400\,m^2s^{-1}$) is located west–northwest of the northern tip of Cape Cod. Elsewhere, diffusivity is on the order of $100\,m^2s^{-1}$. Flow in the deeper areas offshore is generally sluggish compared to the coastal current.

Covariance structures C_{uu} for various nodes off the Cape Cod shoreline illustrate the impact of the coastal geometry and transport fields (Fig. 7). Information on nodes along the northeast coast of Cape Cod (upper two panels) spreads southward with the coastal current. In addition, there is

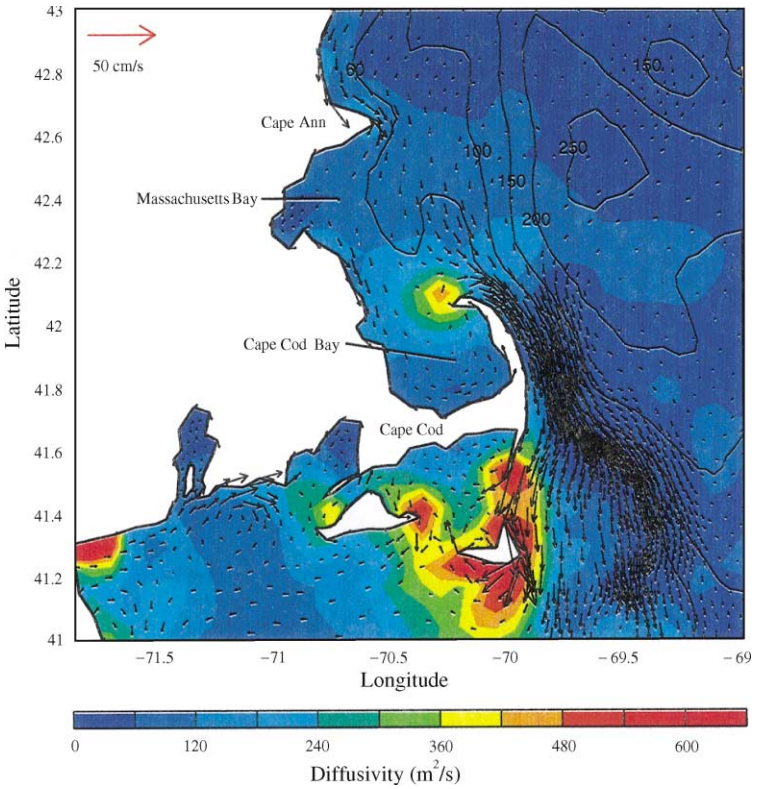

Fig. 6. Climatological velocity and diffusivity fields for the March–April time period. The scale for the velocity vectors appears in the upper left. Selected bathymetric contours are overlayed.

significant propagation of information in the ''upstream'' direction owing to the very high diffusivity present along the northern tip of Cape Cod, with significant covariance penetrating all the way into Cape Cod Bay. In contrast, the covariance structure associated with a node in the southeast corner of Cape Cod Bay is confined to the bay itself, due to the weak currents and low diffusivity present in that region. Similarly, covariance with a node off the southern shore of Cape Cod is limited to Vineyard and Nantucket Sounds. These latter two examples highlight the fact that the coastal geometry is built into the covariance structure, as information clearly does not propagate across land boundaries.

An example Objective Analysis is shown in Fig. 8a. The data are observed concentrations of the toxic dinoflagellate *Alexandrium* spp. from a survey conducted in 1993 as part of the Regional Marine Research Program in the Gulf of Maine. Control parameters for the Objective Analysis (Table 1) were chosen as follows. The observational noise n was set to the precision of the measurement, which is 10 cells l^{-1}. The first-order decay constant k^2 in Eq. (33) sets the horizontal scale of patchiness in the absence of advection and process noise. For a purely diffusive balance ($D\nabla^2 u \sim k^2 u$), the non-dimensional ratio $\sqrt{D}/k$ is the e-folding scale for patches of u. Assuming a typical patch size of 1 km and a diffusivity of $100\,m^2\,s^{-1}$ yields $k^2 = 1.0 \times 10^{-4}$. The process noise is scaled to meet the variance of the observations (d) in the absence of hydrodynamic

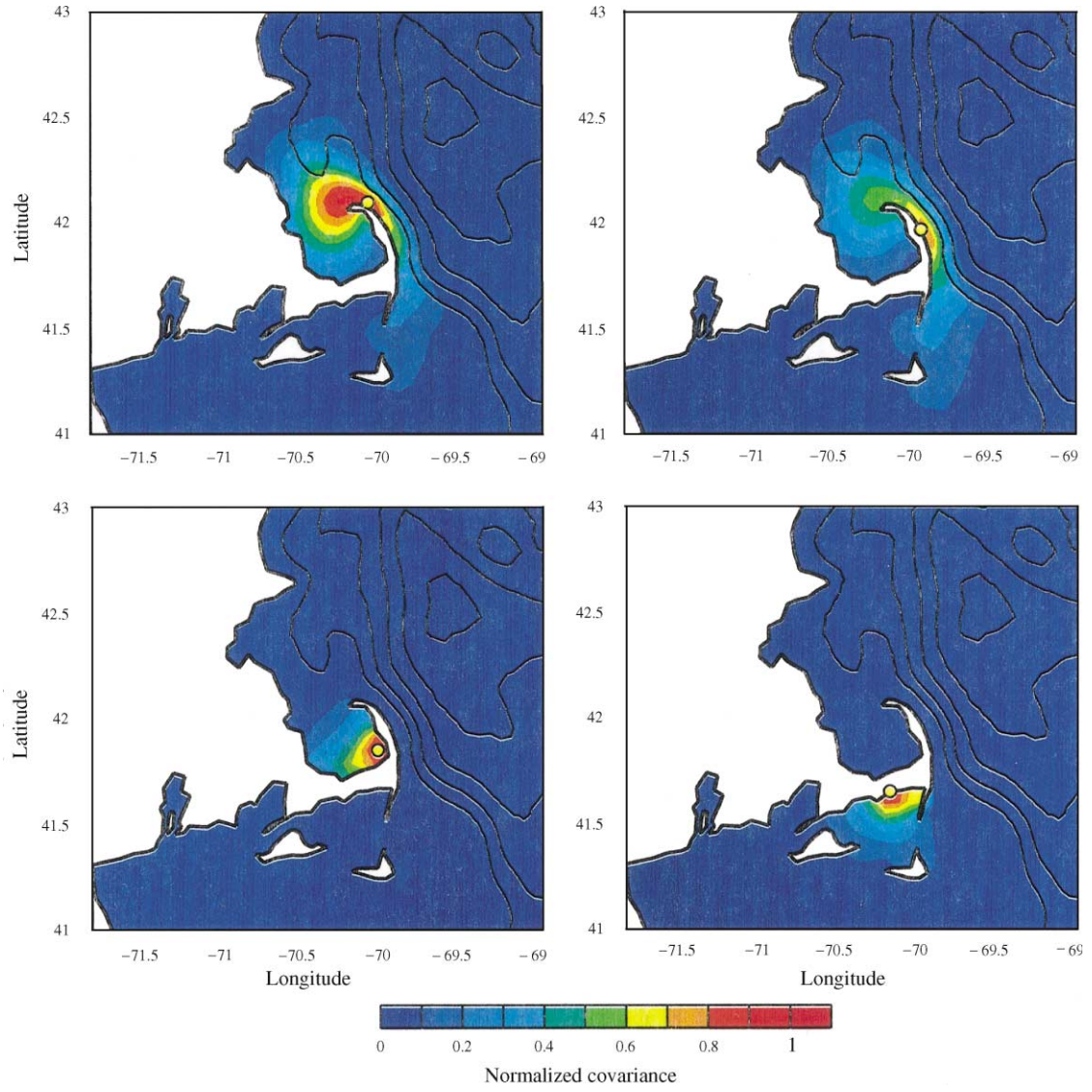

Fig. 7. Normalized covariance structures of four nodes off the Cape Cod shoreline. In each case the covariance is normalized to the value at the node in question (indicated by a white dot). In this example, $k^2 = 2.0 \times 10^{-6}$ and $\varepsilon = 2.0 \times 10^{-6}$. The spatial scale of the process noise is specified to be 2.0×10^3 m.

transport in Eq. (33):

$$Var(\varepsilon) \sim Var(k^2 d).$$

This particular data set has a mean of 92 cells l^{-1} and a standard deviation of 142 cells l^{-1}, resulting in an estimated process noise size $\varepsilon_s = 1.42 \times 10^{-2}$ cells l^{-1} s^{-1}. The covariance of the

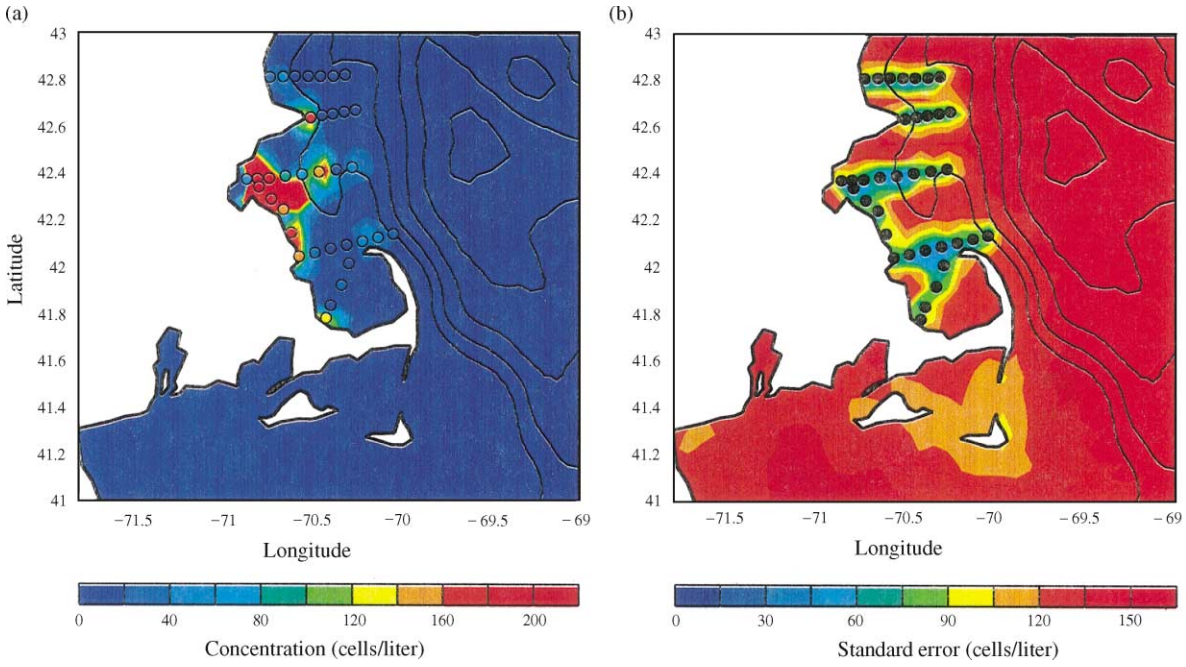

Fig. 8. (a) Objective analysis of *Alexandrium* spp. concentration. Observed values are shown as colored dots, with the same color scale used to map the objectively analyzed field. (b) Standard error estimate, $C_{\tilde{u}\tilde{u}}^{1/2}$.

Table 1
Objective analysis control parameters for Example 2

Parameter	Value	Definition
n	$10\,\text{cells}\,\text{l}^{-1}$	Observational noise
k^2	$1.0 \times 10^{-4}\,\text{s}^{-1}$	First-order decay coefficient
ε	$1.42 \times 10^{-2}\,\text{cells}\,\text{l}^{-1}\,\text{s}^{-1}$	Process noise
r	2 km	Spatial scale of process noise

process noise is assumed to take the form of Eq. (19), with a 2 km spatial scale. The point source noise ε_p was zero.

Although the observed distribution is quite patchy, abundance is generally high in Massachusetts Bay and low elsewhere (Fig. 8a). The objectively analyzed field captures the essence of this pattern, spreading information according to the covariance structure determined by the hydrodynamics and assumptions about the underlying process. Note that the analyzed field does not match the observations exactly; smoothing is implied by the first-order decay specified in Eq. (33), and there is noise associated with both the observations and the process. The accompanying map of standard error (Fig. 8b) is simply the square root of the diagonal of $C_{\tilde{u}\tilde{u}}$. Expected error is reduced in the vicinity of the observations, toward the level of the observational noise. Far from the data, the posterior covariance $C_{\tilde{u}\tilde{u}}$ is no different from the prior covariance

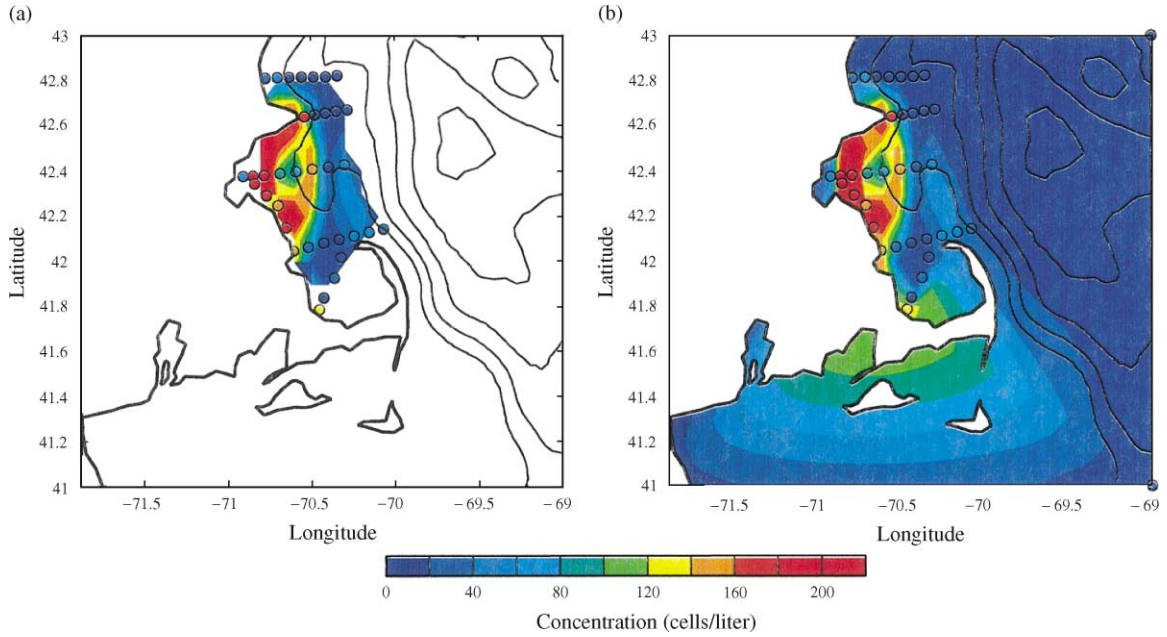

Fig. 9. (a) Cubic interpolation of the same *Alexandrium* spp. concentration data shown in Fig. 8a. Observed values are shown as colored dots. The field is truncated in areas where extrapolation is required. (b) Remapping of (a) in which artificial data points (of zero concentration) are inserted at the corners of the mapping domain in order to force the interpolator to fill the entire field.

C_{uu}. Note that there is structure in the far field standard error. This structure comes as a direct result of the hydrodynamic field. For example, the very high diffusivity near Martha's Vineyard and Nantucket island would tend to smooth any patchiness in that area, thereby reducing the expected variance.

Comparison of these objectively analyzed distributions with maps of the same data made with straightforward interpolation techniques demonstrates the utility of this approach. For example, cubic spline interpolation can be used to fill the gaps in between data points (Fig. 9). With such an algorithm, the resolution of the mesh determines the spatial scale of the interpolated structures. The resulting fields are typically truncated beyond the areas of data coverage (Fig. 9a). Various techniques can be used to force the extrapolation problem, such as the introduction of artificial data points in the far field (e.g., Fig. 9b). However, this ad hoc procedure has obvious shortcomings. The objective analysis technique described herein thus has clear advantages in that it accounts for coastal geometry, a specified hydrodynamic field, and an explicit mathematical representation of the underlying processes assumed to control the distribution of the quantity being mapped.

6. Conclusion

The observational data base for the coastal ocean is growing in sophistication and volume at a remarkable rate. In parallel there is a growing need for state estimation procedures for coastal

fields. Classical Gauss–Markov theory is readily adapted; but knowledge of the prior covariance of the field to be estimated is problematic and potentially limiting. Conventional distance-based covariance functions are not suited to the coastal ocean because of its inhomogeneous nature; but stochastically forced differential equations representing coastal processes provide a natural formulation, and numerical solution is readily obtained with standard finite element procedures. The combination of Gauss–Markov estimation with SDE-based field covariance provides a compact version of coastal OA.[5] It focuses attention on (a) what *processes* are relevant to the observed field variability; and (b) the nature of the stochastic forcing (the *process noise*).

The use of the simple Helmholtz SDE operator provides a locally variable, isotropic correlation scale — in terms of number of grid cells M, we have $M = 1/K \sim [D/k^2A]^{1/2}$, with A the element area. This SDE defaults to conventional distance-based covariance when far from boundaries and inhomogeneities. Adding coastal boundary conditions (no normal transport) blocks interpolation across land. Where a coastal boundary isolates an estimation point from the data, the local estimation error increases. This Helmholtz operator alone is a significant advance over conventional practice. Variation in the diffusion coefficient modulates the correlation scale. Inclusion of an advective term elongates the covariance along streamlines. In the Massachusetts Bays example shown, the climatological circulation and mixing provides a natural specification for these parameters. Even better would be a circulation hindcast of ambient conditions during the cruise.

It is important to pay attention to the spatial correlation in the process noise (ε in Eqs. (21), (29) and (33). Assuming white noise at the nodes of a finite element mesh amounts to large spatial scales where there are big elements—a subtle side effect. In the field application here, we used a distance-based autocorrelation for ε which was successful. Naturally, a large spatial scale for ε overwhelms diffusion and smooths everything. A small spatial scale for ε defaults to the mesh-dependent $[C_{EE}]$ implied by its finite element basis, and allows this to pass through the posterior covariance $[C_{\tilde{u}\tilde{u}}]$. Relative to size, the process noise ought to be scaled to match the observed variance of the data: $Var(\varepsilon) \sim k^2\, Var(d)$. There is substance in the specification of this error model and it deserves careful attention in any analysis.

Boundary conditions for the SDE also warrant attention. We have used homogeneous Neumann BCs which are natural at the coast, with zero variance; these produce a buildup of $[C_{\tilde{u}\tilde{u}}]$, essentially reflecting the covariance. More generally, boundary conditions need to have their own error models explicitly incorporated into the e term in Eqs. (25)–(27).

Two other important OA issues remain unaddressed and should not be overlooked. First, there is the need to describe the observational noise via a relevant error model C_{nn}. We have not looked at this herein, and look forward to the development of error models for the many oceanographic data products becoming available. Second, the data to be analyzed should in general be reduced by removal of a structured prior estimate (spatially-variable mean), in the hope of achieving the zero-mean condition for an unbiased estimate. Explicit recognition of this step is critical to success with any OA procedure.

The Massachusetts Bays application is representative of contemporary shelf modeling; the analyses shown were computed on an office-scale scientific workstation. However the matrices

[5] For an implementation, see the OAFE Users Guide and Software (Lynch and McGillicuddy, 1999).

and inverses involved are, a priori, full; so as computational meshes grow in scope and refinement, these methods may scale unfavorably. To avoid this, it would be practical to reduce the matrix density by truncating the covariance matrices beyond some practical limit, and taking advantage of the resulting sparse matrix structure. Some careful study of this and related ideas is justified, especially in an operational setting.

Acknowledgements

We are grateful to D. Anderson, B. Keafer and R. Signell for providing the *Alexandrium* spp. data used in Figs. 8 and 9. Those data were collected as part of the Regional Marine Research Program for the Gulf of Maine, Project GMR-20. Support for this research was provided through the US ECOHAB program, sponsored by NOAA, NSF, EPA, NASA, and ONR. Additional support was provided by ONR and the US GLOBEC program, sponsored by NSF and NOAA.

This is Contribution #10264 of the Woods Hole Oceanographic Institution; US ECOHAB Contribution #22 and US GLOBEC Contribution #182.

References

Balgovind, R., Dalcher, A., Ghil, M., Kalnay, E., 1983. A stochastic–dynamic model for the spatial structure of forecast error statistics. Monthly Weather Review 111, 701–722.

Bennett, A.F., 1992. Inverse Methods in Physical Oceanography. Cambridge University Press, Cambridge.

Bretherton, F.P., Davis, R.E., Fandry, C.B., 1976. A technique for objective analysis and design of oceanographic experiments applied to MODE-73. Deep Sea Research Part I 23, 559–582.

Daley, R., 1991. Atmospheric Data Analysis. Cambridge University Press, Cambridge.

Denman, K.L., Freeland, H.J., 1985. Correlation scales, objective mapping and a statistical test of geostrophy over the continental shelf. Journal of Marine Research 43, 517–539.

Freeland, H.J., Gould, W.J., 1976. Objective analysis of meso-scale ocean circulation features. Deep Sea Research Part I 23, 915–923.

Gandin, L., 1963. Objective Analysis of Meteorological Fields. Leningrad:Gridromet, English translation 1965. Jerusalem: Israel Program for Scientific Translation.

Hannah, C., Loder, J., Wright, D., 1996. Seasonal variation of the baroclinic circulation in the Scotia Maine region. In: Aubrey, D. (Ed.), Buoyancy Effects on Coastal Dynamics. Coastal and Estuarine Studies, American Geophysical Union, Washington, DC, Vol. 53, pp. 7–29.

Hendry, R., He, I., 2000. Technical report on objective analysis (OA) project. Canadian Technical Report on Hydrog. Ocean Sci., in preparation, http://www.mar.dfo-mpo.gc.ca/science/ocean/coastal_hydrodynamics.oax.html, 2000.

Loder, J., Han, G., Hannah, C., Greenberg, D., Smith, P., 1997. Hydrography and baroclinic circulation in the Scotian Shelf region: winter versus summer. Canadian Journal of Fisheries and Aquatic Sciences 54 (Suppl. 1), 40–56.

Lynch, D.R., Holboke, M.J., Naimie, C.E., 1997. The Maine Coastal Current: spring climatological circulation. Continental Shelf Research 17 (6), 605–634.

Lynch, D.R., Ip, J.T.C., Naimie, C.E., Werner, F.E., 1996. Comprehensive coastal circulation model with application to the Gulf of Maine. Continental Shelf Research 16 (7), 875–906.

Lynch, D.R., McGillicuddy, D.J., 1999. OAFE Users's Guide. http://www-nml.dartmouth.edu/Publications/internal_reports/NML-99-9.

McGillicuddy Jr., D.J., Lynch, D.R., Moore, A.M., Gentleman, W.C., Davis, C.S., Meise, C.J., 1998. An adjoint data assimilation approach to diagnosis of physical and biological controls on *Pseudocalanus* spp. in the Gulf of Maine–Georges Bank region. Fisheries Oceanography 7 (3/4), 205–218.

McWilliams, J.C., 1976. Maps from the Mid-Ocean Dynamics Experiment: Part I. Geostrophic streamfunction. Journal of Physical Oceanography 6, 810–827.

Naimie, C.E., Loder, J.W., Lynch, D.R., 1994. Seasonal variation of the 3-D residual circulation on Georges Bank. Journal of Geophysical Research 99(C8); 15,967–15,989.

Wunsch, C., 1996. The Ocean Circulation Inverse Problem. Cambridge University Press, Cambridge.

Zhou, M., 1998. An objective interpolation method for spatiotemporal distribution of marine plankton. Marine Ecology Progress Series 174, 197–206.